STRUCTURAL BIOLOGY

Insight into structural remodeling of the FlhA ring responsible for bacterial flagellar type III protein export

Naoya Terahara,[1]* Yumi Inoue,[1]* Noriyuki Kodera,[2] Yusuke V. Morimoto,[1,3,4] Takayuki Uchihashi,[2,5,6] Katsumi Imada,[7] Toshio Ando,[2,8] Keiichi Namba,[1,3†] Tohru Minamino[1†]

The bacterial flagellum is a supramolecular motility machine. Flagellar assembly begins with the basal body, followed by the hook and finally the filament. A carboxyl-terminal cytoplasmic domain of FlhA ($FlhA_C$) forms a nonameric ring structure in the flagellar type III protein export apparatus and coordinates flagellar protein export with assembly. However, the mechanism of this process remains unknown. We report that a flexible linker of $FlhA_C$ ($FlhA_L$) is required not only for $FlhA_C$ ring formation but also for substrate specificity switching of the protein export apparatus from the hook protein to the filament protein upon completion of the hook structure. $FlhA_L$ was required for cooperative ring formation of $FlhA_C$. Alanine substitutions of residues involved in $FlhA_C$ ring formation interfered with the substrate specificity switching, thereby inhibiting filament assembly at the hook tip. These observations lead us to propose a mechanistic model for export switching involving structural remodeling of $FlhA_C$.

INTRODUCTION

Biological supramolecular machines assemble in a highly organized and well-controlled manner. One example is the bacterial flagellum, which consist of about 30 different proteins with copy numbers ranging from a few to about 30,000. The flagellum includes at least three parts: the basal body as a rotary motor, the hook as a universal joint, and the filament as a helical propeller. Flagellar assembly begins with the basal body, followed by the hook and finally the filament. There are more than 70 genes in the flagellar regulon of *Salmonella enterica* serovar Typhimurium (hereafter referred to *Salmonella*). Flagellar gene transcription is coupled to the assembly process at the level of completion of hook-basal body (HBB) assembly. During HBB assembly, FlgM, which acts as an anti-σ factor, binds to the flagellum-specific sigma factor σ^{28} to prevent transcription of flagellin gene (*fliC*), stator genes (*motA* and *motB*), chemoreceptor genes (*tar*, *tsr*, etc.), and chemotaxis genes (*che*) that are only required after HBB completion. Upon completion of HBB assembly, a type III protein export apparatus transports FlgM into the culture media, allowing σ^{28} to transcribe these flagellar genes. An export switching machinery allows the protein export apparatus to couple flagellar gene expression with assembly (*1*).

The flagellar export switching machinery consists of at least two flagellar proteins, FliK and FlhB, which act as a molecular ruler and an export switch, respectively, and switches substrate specificity of the flagellar type III protein export apparatus from proteins needed for the structure and assembly of the hook (FlgD, FlgE, and FliK) (hook-type class) to those for the filament assembly (FlgK, FlgL, FlgM, FliC, and FliD) (filament-type class) upon completion of the hook structure to be about 55 nm long in *Salmonella* (*2*). Genetic analysis and photocrosslinking experiments have revealed that an interaction between the C-terminal domain of FliK and the C-terminal cytoplasmic domain of FlhB catalyzes the substrate specificity switch (*3*).

The flagellar type III protein export apparatus is composed of a transmembrane export gate complex made of FlhA, FlhB, FliP, FliQ, and FliR and a cytoplasmic adenosine triphosphatase (ATPase) ring complex consisting of FliH, FliI, and FliJ (*4*, *5*). The protein export apparatus uses adenosine 5′-triphosphate and proton motive force (PMF) across the cytoplasmic membrane as the energy sources and acts as a proton/protein antiporter to couple the proton influx through the gate complex with flagellar protein export (*6*, *7*). FlhA acts as an energy transducer along with the cytoplasmic ATPase ring complex (*6*, *8*, *9*). FlhA forms a homononamer through interactions between its C-terminal cytoplasmic domains ($FlhA_C$) (*10*–*12*). The $FlhA_C$ nonamer acts as the docking platform for FliH, FliI, FliJ, flagellar type III export chaperones, FlgN, FliS, FliT, and export substrates (*2*). $FlhA_C$ consists of domains D1 (residues 362 to 434 and residues 484 to 503), D2 (residues 435 to 483), D3 (residues 504 to 583), and D4 (residues 584 to 682) and a flexible linker termed $FlhA_L$ (residues 328 to 361) (*13*). Filament-type export substrates in complex with their cognate chaperones bind to a highly conserved hydrophobic dimple located at an interface between domans D1 and D2 of $FlhA_C$ to promote unfolding and protein translocation by the protein export apparatus (*14*–*18*). Different binding affinities of $FlhA_C$ for the chaperone-substrate complexes are postulated to ensure the well-defined order of protein export among the filament-type proteins (*16*).

Mutational analysis has shown that a highly conserved cytoplasmic loop between transmembrane helices 4 and 5, which is named the FHIPEP (flagellum/hypersensitive response/invasion protein export pore) domain, coordinates the export of hook-type substrates—FlgD, FlgE, and FliK—with hook assembly (*19*). This suggests that the FHIPEP domain may be part of the entrance gate that regulates well-ordered substrate entry into the pore of the export gate complex. A protonation-mimicking FlhA(D158N) mutation in this FHIPEP domain induces a large conformational change of $FlhA_C$ (*9*). The FHIPEP domain directly binds to $FlhA_C$ (*20*). Because the distance between the cytoplasmic membrane and the $FlhA_C$ ring is about 6 nm (*10*, *11*), it has been proposed that the $FlhA_C$ ring can get close to the FHIPEP domain through a proton-driven conformational change of $FlhA_L$ during protein transport (*9*). Truncations of domain D4 in $FlhA_C$ allow the protein

[1]Graduate School of Frontier Biosciences, Osaka University, 1-3 Yamadaoka, Suita, Osaka 565-0871, Japan. [2]Bio-AFM Frontier Research Center, Kanazawa University, Kanazawa 920-1192, Japan. [3]RIKEN Quantitative Biology Center, 1-3 Yamadaoka, Suita, Osaka 565-0871, Japan. [4]Department of Bioscience and Bioinformatics, Faculty of Computer Science and Systems Engineering, Kyushu Institute of Technology, 680-4 Kawazu, Iizuka, Fukuoka 820-8502, Japan. [5]Department of Physics, Kanazawa University, Kanazawa 920-1192, Japan. [6]Department of Physics, Nagoya University, Chikusa-ku, Nagoya 464-8602, Japan. [7]Department of Macromolecular Science, Graduate School of Science, Osaka University, 1-1 Machikaneyama-cho, Toyonaka, Osaka 560-0043, Japan. [8]Core Research for Evolutional Science and Technology, Japan Science and Technology Agency, Goban-cho, Chiyoda-ku, Tokyo 102-0076, Japan.
*These authors contributed equally to this work.
†Corresponding author. Email: tohru@fbs.osaka-u.ac.jp (T.M.); keiichi@fbs.osaka-u.ac.jp (K.N.)

export apparatus to transport FlgM into the periplasm during HBB assembly (*21*), raising the possibility that the D4 domain may suppress the interactions of $FlhA_C$ with filament-type substrates in complex with their cognate chaperones before HBB completion. However, it remains unknown how the $FlhA_C$ ring undergoes conformational rearrangements to coordinate flagellar protein export with assembly. To clarify this process, we applied high-speed atomic force microscopy (HS-AFM) combined with structure-based functional analyses and provided evidence suggesting that interactions of $FlhA_L$ with the D1 and D2 domains of its neighboring $FlhA_C$ subunit are responsible not only for highly cooperative $FlhA_C$ ring formation but also for the substrate specificity switch.

RESULTS

HS-AFM imaging of the $FlhA_C$ ring structure

$FlhA_C$ stably exists as a monomer in solution even at high protein concentrations (*22*) although it is directly involved in FlhA ring formation in vivo (*10*, *12*). To clarify how $FlhA_C$ facilitates ring formation, we purified $FlhA_C$ monomers by size-exclusion chromatography (fig. S1A) and observed structural dynamics of $FlhA_C$ at a single molecular level by HS-AFM, which is able to visualize protein complexes in action at a high spatiotemporal resolution (*23*–*25*). The molecular shape of the $FlhA_C$ monomer in the experimental AFM image was almost the same as that of a simulated image constructed from the crystal structure of *Salmonella* $FlhA_C$ (fig. S1B) (*13*). $FlhA_C$ monomers associated with and dissociated from each other and finally formed a stable ring-shaped structure (Fig. 1A and movie S1). The shape of the $FlhA_C$ ring in the experimental AFM image was almost the same as that of a simulated image constructed from the nonameric ring model of *Salmonella* $FlhA_C$ (Fig. 1B and movie S2) (*11*). About 80% of $FlhA_C$ rings contained nine copies of $FlhA_C$ subunits ($n = 100$) (Fig. 1C), in agreement with previous reports (*10*–*12*). The diameter (peak-to-peak distance) and the height of the $FlhA_C$ ring were estimated to be 10.1 ± 0.6 nm and 5.1 ± 0.4 nm, respectively (Fig. 1, D and E), which are almost the same as those of the three-dimensional density map of the in situ $FlhA_C$ ring structure (*10*, *11*). Therefore, we conclude that this AFM image of the $FlhA_C$ ring reflects the in vivo structure. The number of the $FlhA_C$ ring was considerably increased with an increase in protein concentration (Fig. 1F and fig. S2A). The dissociation constant and the Hill's cooperativity coefficient were estimated to be about 0.72 ± 0.02 μM and 5.5 ± 0.8, respectively. These suggest that $FlhA_C$ forms a homononamer in a highly cooperative manner.

Effect of a deletion of $FlhA_L$ on $FlhA_C$ ring formation

Two $FlhA_C$ molecules are present in an asymmetric unit of the *Salmonella* $FlhA_C$ crystal (Fig. 2A), and the molecules form a tubular structure with a left-handed 8_1 screw symmetry along the *c* axis in the crystal (*13*). $FlhA_L$ consists of residues 328 to 361 (*13*, *22*). In the crystal structure, the N-terminal 19 residues of $FlhA_L$ (328 to 346, $FlhA_{L\text{-}N}$) are invisible and the following 15 residues (347 to 361, $FlhA_{L\text{-}C}$) bind to the D1 and D3 domains of its neighboring subunit along the 1-start helix (Fig. 2A) (*13*). This raises the possibility that $FlhA_{L\text{-}C}$ contributes to highly cooperative $FlhA_C$ ring formation. To test this hypothesis, we first purified $FlhA_C$ monomers lacking residues 328 to 351 of FlhA ($FlhA_C$38K) (*22*) and used HS-AFM to analyze the capability of these monomers for ring formation. $FlhA_C$38K monomers interacted with and dissociated from each other in a way similar to wild-type $FlhA_C$ but did not form the ring-like structure (Fig. 2B and movie S3), indicating that residues 328 to 351 of $FlhA_L$ are required for stable ring formation on mica surface. Because $FlhA_C$ can get close to the cytoplasmic surface of the cytoplasmic membrane when it interacts with the FHIPEP domain of FlhA (*9*, *20*), we next investigated whether phospholipids affect $FlhA_C$ ring formation. We spread planar phospholipid bilayers on mica surface, placed a solution sample of wild-type $FlhA_C$ monomers or $FlhA_C$38K monomers with various concentrations, and analyzed their ring formation. Wild-type $FlhA_C$ also formed the nonameric ring structure on mica-supported planar phospholipid bilayers in a protein concentration–dependent manner (Fig. 2B, fig. S2B, and movie S4). The dissociation constant and the Hill's cooperativity coefficient were estimated to be about 2.3 ± 0.01 μM and 7.4 ± 0.2, respectively (Fig. 2C), indicating that phospholipids enhance positively cooperative ring formation but reduce the binding affinity for its nearest neighboring subunit. Phospholipids stabilized interactions between $FlhA_C$38K monomers to a considerable degree, facilitating the formation of the ring-shaped structure on the mica-supported planar phospholipid bilayers (Fig. 2B, fig. S2C, and movie S5). The dissociation constant and the Hill's cooperativity coefficient were estimated to be about 10.3 ± 0.8 μM and 2.2 ± 0.4, respectively (Fig. 2C), indicating that residues 328 to 351 of $FlhA_L$ are required for highly cooperative ring formation of $FlhA_C$. Because the D1-D3 and D3-D3 interactions mainly contribute to $FlhA_C$ ring formation (*10*), we conclude that $FlhA_L$ stabilizes these two interactions through interactions of $FlhA_{L\text{-}C}$ with the D1 and D3 domains of its neighboring $FlhA_C$ subunit.

Effects of alanine substitutions of residues involved in interactions of $FlhA_L$ with its neighboring subunit on flagellar assembly

Two negatively charged residues, Glu^{351} and Asp^{356}, in $FlhA_{L\text{-}C}$ bind to a positively charged cluster formed by Arg^{388}, Arg^{391}, Lys^{392}, and Lys^{393} in domain D1 of its neighboring subunit in the crystal. Trp^{354} in $FlhA_{L\text{-}C}$ binds to a hydrophobic pocket formed by Val^{357} of $FlhA_{L\text{-}C}$ and Phe^{400} and Leu^{401} in domain D1, Leu^{512} in domain D3, and the side chain arms of Glu^{508}, Gln^{511}, and Arg^{515} in domain D3 of its neighboring subunit (Fig. 2A). Glu^{351} is missing in $FlhA_C$38K, raising the possibility that these residues are responsible for highly cooperative $FlhA_C$ ring formation on mica. To clarify the role of these residues, we introduced the W354A, E351A/D356A, E351A/W354A/D356A, R391A/K392A/K393A, L401A, and Q511A mutations into FlhA by site-directed mutagenesis. Immunoblotting with polyclonal anti-$FlhA_C$ antibody revealed that these mutations did not affect the protein stability of FlhA (fig. S3A). To test whether these mutations affect FlhA function, we analyzed the effect of these substitutions on motility in soft agar (fig. S3B). FlhA(Q511A) fully restored motility of the Δ*flhA* mutant. In agreement with this, the Q511A mutation affected neither flagellar protein export nor assembly at all (Fig. 3A, lane 16, and fig. S3C), indicating that Gln^{511} is not essential for the FlhA function. FlhA(L401A) restored the motility to a considerable degree although not to the wild-type level. The W354A and E351A/D356A mutants complemented the Δ*flhA* mutant to some degree, and the E351A/W354A/D356A and R391A/K392A/K393A mutants did not at all (fig. S3B). Consistently, the W354A and E351A/D356A mutants produced only a few flagellar filaments, of which length was much shorter than the wild-type length, and the E351A/W354A/D356A and R391A/K392A/K393A mutants produced no flagellar filaments (fig. S3C). These results indicate that Trp^{354}, Glu^{351}, Asp^{356}, Arg^{391}, Lys^{392}, and Lys^{393} are involved in flagellar formation.

To test how these FlhA mutations affect flagellar assembly, we analyzed the secretion levels of hook-type proteins (FlgD and FlgE) and

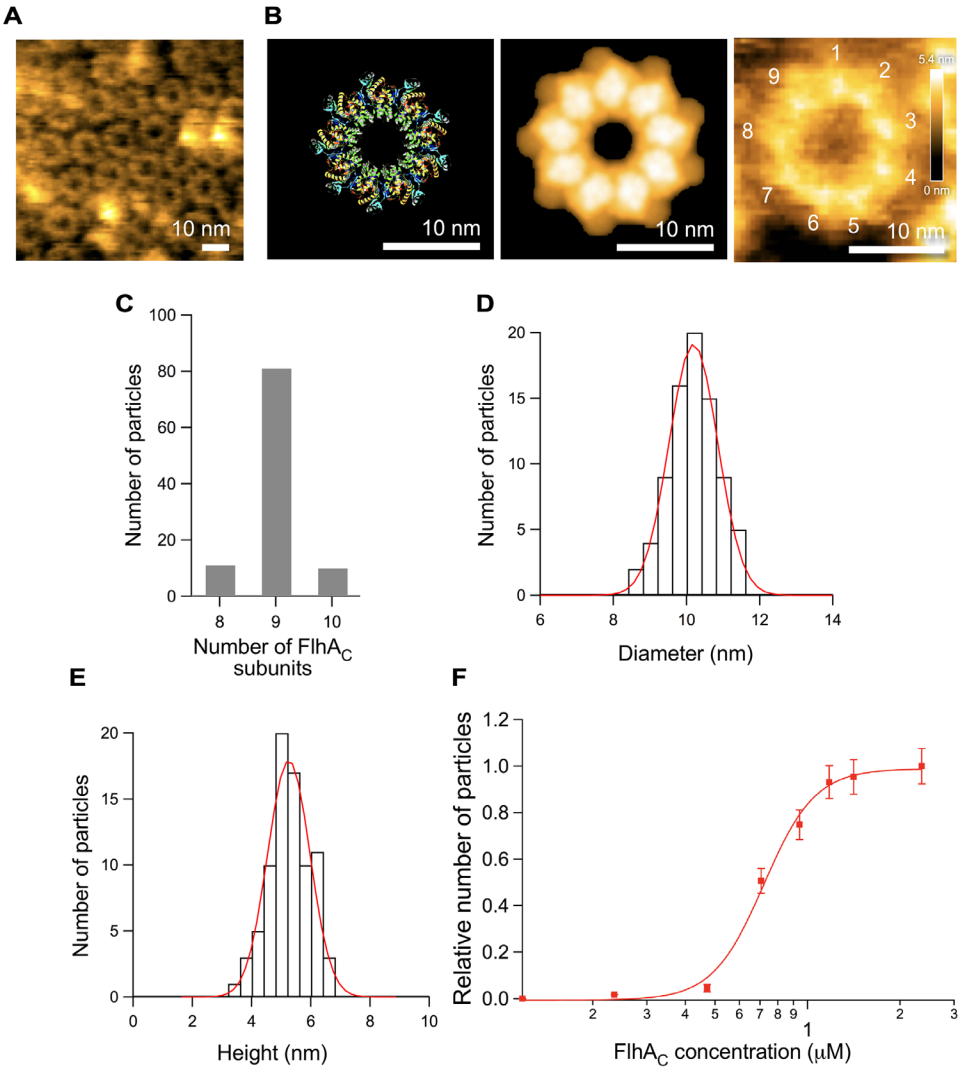

Fig. 1. FlhA$_C$ forms a ring-shaped structure. (**A**) Typical HS-AFM image of FlhA$_C$ placed on mica at a protein concentration of 2.4 μM. The image was recorded at 200 ms per frame in a scanning area of 100 × 100 nm^2 with 100 × 100 pixels. (**B**) Comparison of a simulated HS-AFM image (middle panel) constructed from the atomic model of the FlhA$_{C9}$ ring structure (left panel) with an experimental HS-AFM image of the FlhA$_C$ ring (right panel) obtained at a concentration of 0.71 μM. The HS-AFM image was recorded at 200 ms per frame in a scanning area of 50 × 50 nm^2 with 100 × 100 pixels. Color bar shows a range of particle height (nanometers). (**C** to **E**) Histograms of the stoichiometry (C), diameter (peak-to-peak distance), (D) and height (E) of the FlhA$_C$ ring. (**F**) Effect of protein concentrations on FlhA$_C$ ring formation. Ring particles per frame were counted under each condition. The number of the ring formed at the highest protein concentration is set to 1. Relative ring particle numbers versus protein concentrations (micromolar) are plotted and fitted by Hill equation.

filament-type proteins (FlgM, FlgK, FlgL, and FliC). The W354A, E351A/D356A, and R391A/K392A/K393A mutants secreted both FlgD and FlgE almost at the wild-type levels (Fig. 3A, lanes 11, 12, and 14) and so produced HBBs (Fig. 3B). These results indicate that the W354A, E351A/D356A, and R391A/K392A/K393A mutations do not inhibit HBB assembly. Their hook length distributions were quite broad compared to the wild-type (fig. S3D). The R391A/K392A/K393A mutant produced much longer hooks called polyhooks (Fig. 3B). These observations suggest that these mutations affect the hook length control significantly. In contrast, the W354A, E351A/D356A, and R391A/K392A/K393A mutations inhibited the secretion of FlgM, FlgK, FlgL, and FliC (Fig. 3A, lanes 11, 12, and 14). In addition, the cellular expression levels of FliC were much lower in these *flhA* mutants than the wild-type level (Fig. 3A, sixth row, lanes 3, 4, and 6). FlgM acts as an anti-σ factor to inhibit the transcription of *fliC* during HBB assembly. Upon hook completion, the flagellar type III protein export apparatus secretes FlgM into the culture media, allowing FliC to be expressed, exported, and assembled into the filament at the tip of the hook-filament junction made of FlgK and FlgL with the help of the FliD cap (*26*). Therefore, we suggest that the W354A, E351A/D356A, and R391A/K392A/K393A mutations interfere with substrate specificity switching of the flagellar export apparatus from the hook-type to the filament-type. Neither hook-type nor filament-type substrates were secreted by the E351A/W354A/D356A mutant (Fig. 3A, lane 13), and so, only the MS-C rings were produced (Fig. 3B). This indicates that the E351A/W354A/D356A triple mutation abolishes the PMF-driven flagellar protein export process.

The *flhA*(L401A) mutant cells secreted FlgD and FlgE into the culture media at wild-type levels (Fig. 3A, lane 15) and produced hooks with normal length distribution (Fig. 3B). In contrast, the levels of FlgM,

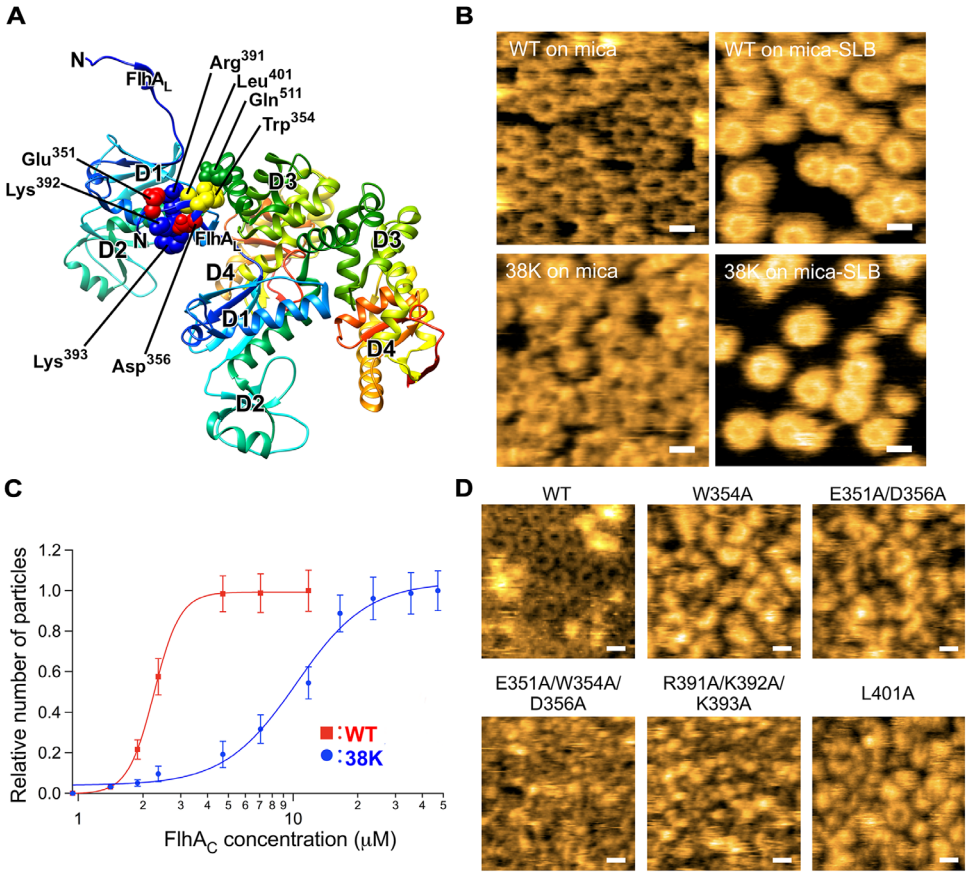

Fig. 2. Effect of deletion of residues 328 to 351 in FlhA$_L$ on FlhA$_C$ ring formation. (**A**) Crystal structure of the FlhA$_C$ dimer [PDB (Protein Data Base) ID: 3A5I]. FlhA$_C$ contains four domains, D1, D2, D3, and D4, and a flexible linker termed FlhA$_L$. The asymmetric unit of the crystal contains two FlhA$_C$ molecules. Residues 347 to 361 of FlhA$_L$ bind to the D1 and D3 domains of its neighboring subunit. Residues involved in this interaction are shown. The Cα backbone is color-coded from blue to red, going through the rainbow colors from the N terminus to the C terminus. (**B**) Typical HS-AFM images of wild-type FlhA$_C$ (indicated as WT) and FlhA$_C$38K (indicated as 38K) lacking residues 328 to 351 of FlhA$_L$ placed either on mica or mica-supported planar phospholipid bilayer (mica-SLB). The protein concentrations were ca. 2.4 and 11.8 μM when they were placed on the mica and phospholipid surfaces, respectively. The HS-AFM images on the mica surface were recorded at 200 ms per frame in a scanning area of 100 × 100 nm^2 with 150 × 150 pixels. The images on phospholipids were recorded at 500 ms per frame in a scanning area of 100 × 100 nm^2 with 200 × 200 pixels. Scale bars, 10 nm. (**C**) Effect of protein concentrations on FlhA$_C$ ring formation on phospholipid bilayer. Ring particles per frame were counted under each condition. Relative ring particle numbers versus protein concentrations (micromolar) are plotted and fitted by Hill equation. (**D**) Typical HS-AFM images of wild-type FlhA$_C$ and its mutant variants, W354A, E351A/D356A, E351A/W354A/D356A, R391A/K392A/K393A, and L401A placed on a mica surface at a concentration of 2.4 μM. All images were recorded at 200 ms per frame in a scanning area of 100 × 100 nm^2 with 150 × 150 pixels. Scale bars, 10 nm.

FlgK, FlgL, and FliC secreted by the L401A mutant were only 50% of wild-type levels (Fig. 3A, lane 15). Because the *flhA*(L401A) mutant formed filaments at wild-type levels when grown overnight at 30°C (fig. S3C), this suggests that the FlhA(L401A) mutation reduces the rate of filament polymerization. Because the W354A, E351A/D356A, and R391A/K392A/K393A mutants produced longer hooks without the filament attached, we propose that Glu^{351}, Trp^{354}, and Asp^{356} in FlhA$_{L\text{-}C}$ and Arg^{391}, Lys^{392}, and Lys^{393} in domain D1 are responsible for the substrate specificity switching of the flagellar export apparatus upon completion of HBB assembly.

Effects of alanine substitutions of residues involved in interactions of FlhA$_L$ with its neighboring subunit on FlhA$_C$ ring formation

To investigate whether Glu^{351}, Trp^{354}, Asp^{356}, Arg^{391}, Lys^{392}, and Lys^{393} are also responsible for FlhA$_C$ ring formation, we analyzed the effect of alanine substitutions of these residues on FlhA$_C$ ring formation by HS-AFM. The W354A, E351A/D356A, E351A/W354A/D356A, and R391A/K392A/K393A mutations inhibited FlhA$_C$ ring formation on mica even at high protein concentrations, although intermediate ring structures were observed frequently (Fig. 2D). Unlike FlhA$_C$38K lacking residues 328 to 351, planar phospholipid bilayers did not improve their capability of ring formation even at high protein concentrations (fig. S4). These results indicate that these mutations significantly affect the D1-FlhA$_{L\text{-}C}$ and D3-FlhA$_{L\text{-}C}$ interactions. Because FlhA$_C$38K retains the ability to form the nonameric ring structure to a considerable degree in the presence of phospholipids (Fig. 2B), this raises the possibility that FlhA$_{L\text{-}N}$ regulates highly cooperative FlhA$_C$ ring formation. The FlhA(L401A) mutant variant retained the ability to form the nonameric ring structure to some degree only when a protein concentration was high enough (Fig. 2D and fig. S4). Therefore, we suggest that the interactions of FlhA$_{L\text{-}C}$ with the D1 and D3 domains of its neighboring subunit are responsible for FlhA$_C$ ring formation in a highly cooperative manner.

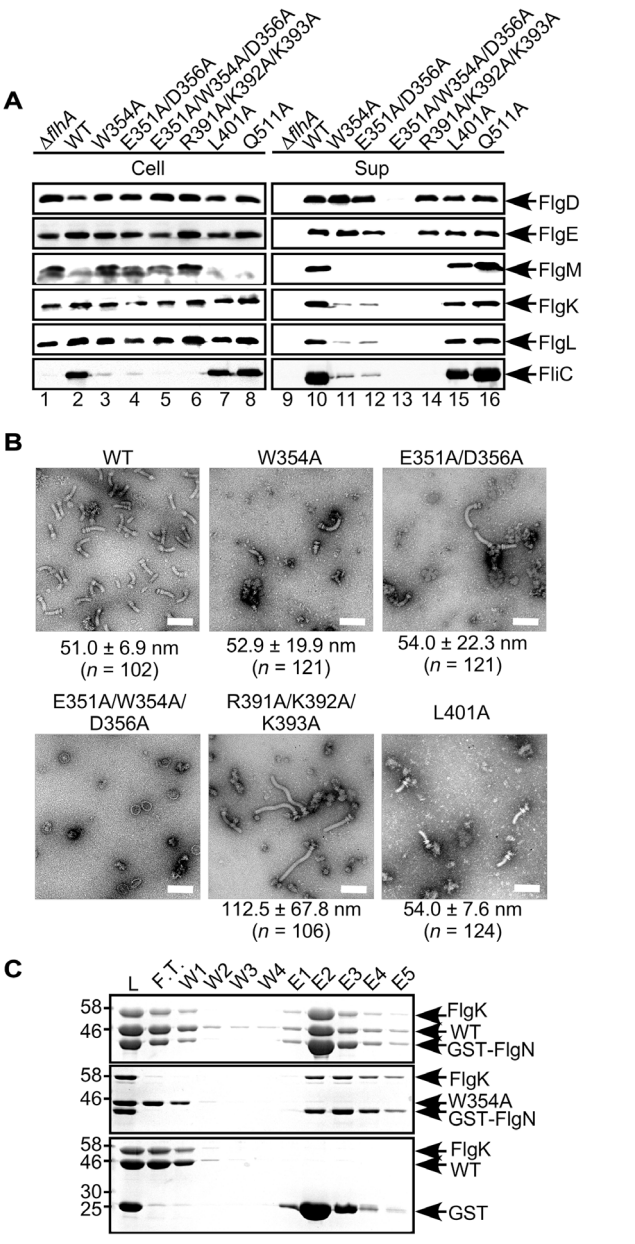

Fig. 3. Effect of alanine substitutions of residues involved in interactions of $FlhA_L$ with its neighboring subunit on FlhA function. (**A**) Secretion assays of flagellar proteins. Immunoblotting using polyclonal anti-FlgD (first row), anti-FlgE (second row), anti-FlgM (third row), anti-FlgK (fourth row), anti-FlgL (fifth row), or anti-FliC (sixth row) antibody, of whole-cell proteins (Cell) and culture supernatants (Sup). Lanes 1 and 9, Δ*flhA*; lanes 2 and 10, wild-type (WT); lanes 3 and 11, *flhA*(W354A) (W354A); lanes 4 and 12, *flhA*(E351A/D356A) (E351A/D356A); lanes 5 and 13, *flhA*(E351A/W354A/D356A) (E351A/W354A/D356A); lanes 6 and 14, *flhA*(R391A/K392A/K393A) (R391A/K392A/K393A); lanes 7 and 15, *flhA*(L401A) (L401A); and lanes 8 and 16, *flhA*(Q511A) (Q511A). The positions of FlgD, FlgE, FlgM, FlgK, FlgL, and FliC are indicated by arrows. (**B**) Electron micrograms of HBB isolated from the above stains. The average hook length and SDs are shown. Scale bars, 100 nm. (**C**) Interaction between $FlhA_C$ and FlgN-FlgK complex. Purified His-$FlhA_C$ (WT) or His-$FlhA_C$(W354A) (W354A) was mixed with GST-FlgN in complex with FlgK (first and second rows), or GST alone (third row) and dialyzed overnight against phosphate-buffered saline (PBS) and dialyzed overnight against PBS. The mixture (L) was subjected to GST affinity chromatography. Flow through fraction (F.T.), wash fractions (W), and elution fractions (E) were analyzed by CBB (Coomassie brilliant blue) staining.

Effects of FlhA mutations on interactions of $FlhA_C$ with FlgN and FliJ

The FlgN-FlgK, FlgN-FlgL, FliT-FliD, and FliS-FliC chaperone-substrate complexes directly bind to $FlhA_C$ through interactions of FlgN, FliT, and FliS with a highly conserved hydrophobic dimple at an interface between domains D1 and D2 of $FlhA_C$ (*14*–*18*). We found that the W354A, E351A/D356A, R391A/K392A/K393A, and L401A mutations significantly reduced the export of FlgK, FlgL, and FliC, raising the question of whether these mutations affect the interactions of $FlhA_C$ with the chaperone-substrate complexes. To clarify this possibility, we carried out pull-down assays by glutathione *S*-transferase (GST) affinity chromatography. $FlhA_C$ copurified with GST-FlgN in complex with FlgK and GST-FlgN alone but not with GST alone (Fig. 3C and fig. S5A), in agreement with previous reports (*15*, *16*). In contrast, the W354A, E351A/D356A, R391A/K392A/K393A, and L401A mutant variants did not copurify with the GST-FlgN–FlgK complex and GST-FlgN (Fig. 3C and fig. S5A). Because these mutations inhibit $FlhA_C$ ring formation even in the presence of phospholipids, this suggests that the interaction site for the FlgN-FlgK complex may lie across more than one subunit in the $FlhA_C$ ring structure. Because Tyr^{122} of FlgN, which is highly conserved among FlgN homologs, interacts with Asp^{456}, Phe^{459}, and Thr^{490} in the conserved hydrophobic dimple of $FlhA_C$ (*15*), it is also possible that these mutations could affect a conformation of this conserved hydrophobic dimple, thereby reducing the binding affinities of $FlhA_C$ for FlgN significantly.

$FlhA_L$ is directly involved in the interaction with FliJ (*6*, *14*). Therefore, we tested whether the FlhA mutations also reduce the binding affinity of FlhA for FliJ. Wild-type FlhA copurified with GST-FliJ but not with GST alone (Fig. 4A and fig. S5B), in agreement with a previous report (*6*). Except for the Q511A mutant, which displayed no phenotype (fig. S3), the other mutations significantly reduced the binding affinity of FlhA for FliJ (Fig. 4A). Consistently, the W354A, E351A/D356A, E351A/W354A/D356A, R391A/K392A/K393A, and L401A mutations inhibited the interaction between $FlhA_C$ and FliJ (fig. S5C). These results suggest that Glu^{351}, Trp^{354}, Asp^{356}, Arg^{391}, Lys^{392}, Lys^{393}, and Leu^{401} are required for the interaction with FliJ.

It has been shown that an interaction between FliJ and $FlhA_L$ is critical for PMF-driven flagellar protein export and that FliH and FliI ensure the FliJ-$FlhA_L$ interaction to allow the export gate complex to efficiently transport flagellar proteins in a PMF-dependent manner (*6*, *27*). Unlike a *Salmonella flhA* mutant lacking residues 328 to 351 of $FlhA_L$ that cannot transport any flagellar proteins (*22*), we found that the W354A, E351A/D356A, R391A/K392A/K393A, and L401A mutants produced HBBs at the wild-type level, raising the possibility that FliH and FliI also support the FliJ-$FlhA_L$ interaction to induce conformational rearrangements of $FlhA_C$ responsible for the substrate specificity switch. We found that the FlhA(L401A) mutation reduced not only the rates of filament-type protein export but also the binding affinity of $FlhA_C$ for FliJ, whereas the FlhA(Q511A) mutation did not at all (Figs. 3 and 4A). This raises the possibility that FlhA(L401A) probably requires the support of FliH and FliI to exert its export activity to a considerable degree, whereas FlhA(Q511A) does not. To test this hypothesis, we used a Δ*fliH-fliI flhB*(P28T) (Δ*fliH-fliI flhB**) mutant, of which second-site P28T mutation in FlhB considerably increases the probability of flagellar protein export and assembly in the absence of FliH and FliI (*28*). FlhA(Q511A) restored motility of the *Salmonella* Δ*fliH-fliI flhB** Δ*flhA* mutant to the wild-type level, whereas FlhA (L401A) did not (Fig. 4B, upper panel). The Δ*fliH-fliI flhB** *flhA* (Q511A) mutant secreted both FlgD and FlgK at the wild-type levels

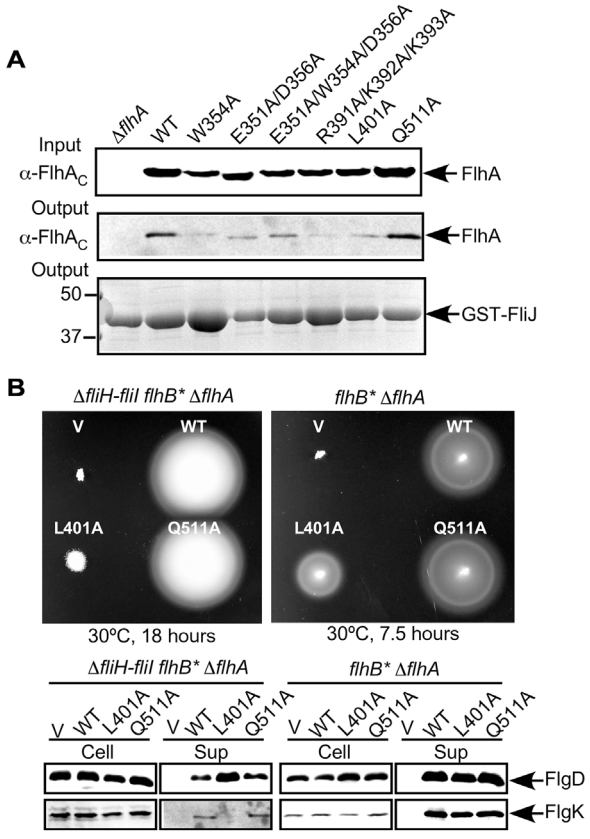

Fig. 4. Effect of depletions of FliH and FliI on the export function of FlhA(L401A). (**A**) Interaction between FliJ and FlhA$_C$. The mixture of the soluble fractions (Input) prepared from *Salmonella* Δ*flhDC-cheW* cells expressing GST-FliJ with those from a *Salmonella* Δ*flhA* mutant carrying pTrc99AFF4 (indicated as Δ*flhA*), pMM130 (WT), pYI001 (W354A), pYI002 (E351A/D356A), pYI003 (E351A/W354A/D356A), pYI004 (R391A/K392A/K393A), pYI005 (L401A), or pYI006 (Q511A) was loaded onto a GST column. After extensive washing, proteins were eluted with a buffer containing 10 mM reduced glutathione. The eluted fractions were analyzed by immunoblotting with polyclonal anti-FlhA antibody (first and second rows) and CBB staining for GST-FliJ (third row). (**B**) Motility of and flagellar protein export by NH004 (Δ*fliH-fliI flhB** Δ*flhA*) (left panel) and NH002 (*flhB** Δ*flhA*) (right panel) harboring pTrc99AFF4 (V), pMM130 (WT), pYI005 (L401A), or pYI006 (Q511A). Upper panels: Motility assays in soft agar at 30°C. Lower panels: Immunoblotting, using polyclonal anti-FlgD and anti-FlgK antibodies, of whole-cell proteins (Cell) and culture supernatant fractions (Sup).

(Fig. 4B, lower panel). In contrast, the Δ*fliH-fliI flhB** *flhA*(L401A) mutant secreted a much higher amount of FlgD into the culture media compared to the wild-type level but not FlgK at all (Fig. 4B, lower panel). Consistently, the Δ*fliH-fliI flhB** *flhA*(L401A) cells produced HBBs (fig. S6A). We obtained essentially the same results with the Δ*fliH flhA* (L401A) and Δ*fliH-fliI flhA*(L401A) mutants (fig. S6B). When FliH and FliI were expressed in the Δ*fliH-fliI flhB** *flhA*(L401A) cells, motility was restored considerably (Fig. 4B, upper panel). In agreement with this, FlgK was secreted into the culture media (Fig. 4B, lower panel). These results indicate that FlhA(L401A) requires FliH and FliI to exert its export activity. Therefore, we propose that an interaction between FliJ and FlhA$_C$, which is ensured by FliH and FliI, may induce structural remodeling of the FlhA$_C$ ring upon completion of HBB assembly, allowing the flagellar type III protein export apparatus to initiate the export of filament-type proteins to form the filament at the hook tip.

Effects of the FlhA(F459A) mutation on FlhA$_C$ ring formation

The FlhA(F459A) mutation, which is located in a conserved hydrophobic dimple at an interface between domains D1 and D2 of FlhA$_C$, reduces the binding affinities of FlhA$_C$ for the FlgN-FlgK, FlgN-FlgL, FliT-FliD, and FliS-FliC complexes (*15*, *16*). As a result, the secretion levels of FlgK, FlgL, FliD, and FliC are reduced significantly, although the F459A mutation does not affect hook-type protein export at all (*16*, *29*). The *flhA*(F459A) mutant phenotype looks similar to that of the *flhA*(L401A) mutant, raising the possibility that the FlhA(F459A) mutation might affect the interaction with FliJ. The *flhA*(F459A) mutant produced normal hooks with nearly normal average length and length distribution (fig. S7A), in agreement with a previous report (*29*). Pull-down assays by GST affinity chromatography revealed that the F459A mutation did not weaken the interaction of FlhA$_C$ with FliJ (fig. S7B). HS-AFM imaging revealed that FlhA$_C$(F459A) formed a nonameric ring structure with 9.8 ± 0.5 nm in diameter (peak-to-peak distance) and 5.0 ± 0.4 nm in height in a way similar to wild-type FlhA$_C$ (fig. S7, C to F). These results indicate that the F459A mutation affects neither the interaction of FlhA$_C$ with FliJ nor FlhA$_C$ ring formation. Therefore, we conclude that Phe^{459} is directly involved in the interaction with the flagellar export chaperone-substrate complexes.

DISCUSSION

The flagellar type III protein export apparatus switches its substrate specificity from the hook-type to the filament-type. FliK and FlhB are responsible for this switching event (*1*, *2*). FlhA forms a homononamer through interactions between FlhA$_C$ domains at the flagellar base (*10*–*12*). FlhA$_C$, which consists of domains D1, D2, D3, and D4 and FlhA$_L$ (*13*), coordinates flagellar protein export with assembly (*16*, *21*). However, little is known about FlhA$_C$ action. The crystal structure of the C-terminal cytoplasmic domain of MxiA (MxiA$_C$), which is an FlhA homolog of the *Shigella* virulence-associated type III secretion apparatus, forms a nonameric ring through D1-D3 and D3-D3 interactions (*10*). Although *Salmonella* FlhA$_C$ does not form such a ring structure in the crystal, very similar interactions between FlhA$_C$ molecules are observed (Fig. 2A) (*13*). Here, real-time imaging by HS-AFM revealed that *Salmonella* FlhA$_C$ forms a nonameric ring structure on mica surface in a highly cooperative manner and that FlhA$_L$ is required for efficient FlhA$_C$ ring formation (Figs. 1 and 2). Alanine substitutions of Glu^{351}, Trp^{354}, and Asp^{356} in FlhA$_{L\text{-}C}$ and Arg^{391}, Lys^{392}, and Lys^{393} in domain D1, which are involved in the interaction of FlhA$_L$ with its neighboring FlhA$_C$ subunit in the FlhA$_C$ crystal (Fig. 2A) (*13*), not only inhibited cooperative FlhA$_C$ ring formation on both mica and phospholipids (Fig. 2D) but also reduced the probability of filament assembly upon completion of HBB assembly (Fig. 3A and fig. S3). These mutations also reduced the binding affinity of FlhA$_C$ for the FlgN chaperone, thereby reducing the export of FlgK and FlgL considerably (Fig. 3 and fig. S5A). This raises the possibility that the interaction site for the FlgN-FlgK complex lies across more than one subunit in the FlhA$_C$ ring structure. Because the W354A, E351A/D356A, and R391A/K392A/K393A mutants produced the HBBs at the wild-type level (Fig. 3B), we suggest that the interactions of FlhA$_L$ with its neighboring subunit in the ring structure initiate the export of filament-type proteins upon HBB completion (Fig. 5). A highly conserved hydrophobic dimple at an interface between domains D1 and D2 of FlhA$_C$ provides a binding site for flagellar export chaperone-substrate complexes (*14*–*16*). A well-conserved Phe^{459} residue in the hydrophobic dimple is directly involved in the interaction

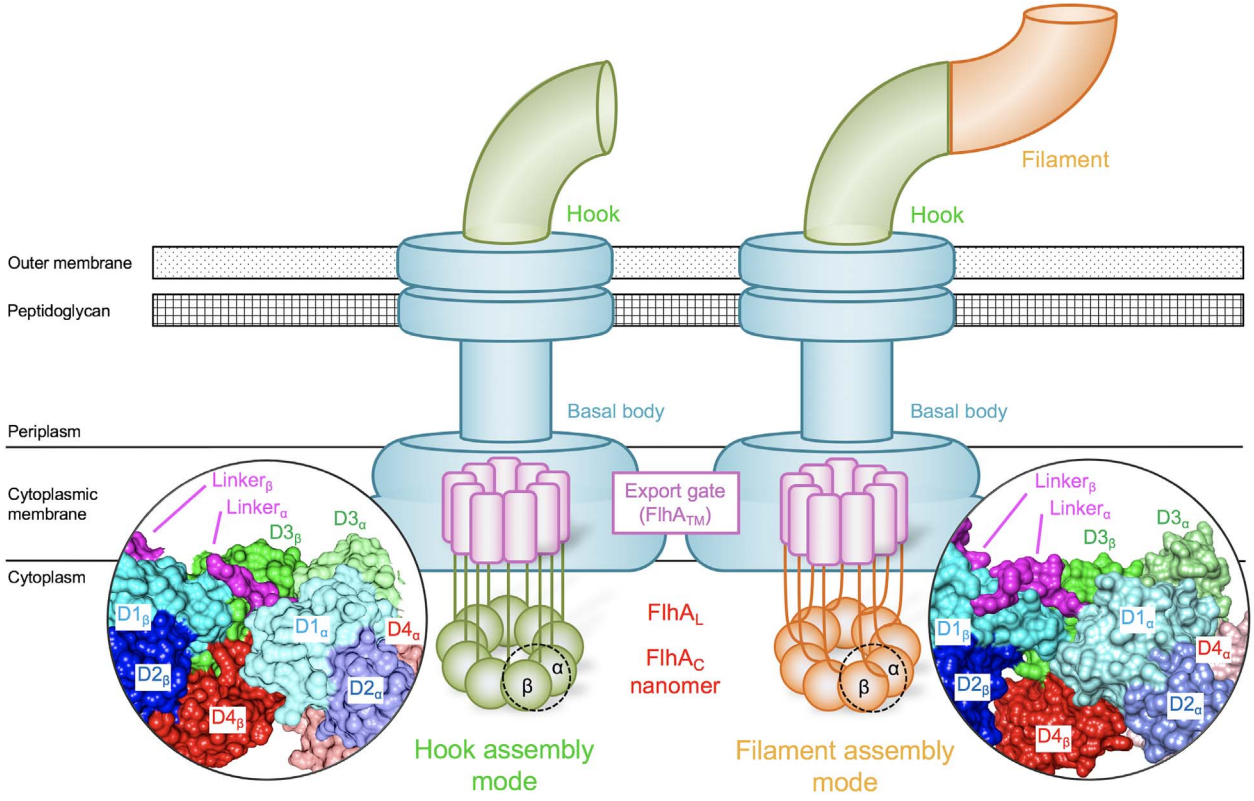

Fig. 5. Model for cooperative remodeling of the FlhA$_C$ ring structure. Partial atomic models of the MxiA$_C$ (left; PDB ID: 4A5P) and FlhA$_C$ (right; PDB ID: 3A5I) ring models are shown. Both MxiA$_C$ and FlhA$_C$ consist of domains D1 (cyan), D2 (blue), D3 (light green), and D4 (red). FlhA$_C$ forms a nonameric ring structure mainly through interactions between D3 domains and between domains D1 and D3. Only an N-terminal short stretch forming part (magenta) of a flexible linker is visible, whereas most of residues forming the linker are invisible because of their conformational flexibility. In contrast, about a C-terminal half of FlhA$_L$ binds to its neighboring subunit in the FlhA$_C$ crystal. During hook assembly, FlhA$_L$ does not bind to its neighboring subunit, allowing the flagellar type III protein export apparatus to transport the hook protein. Upon completion of the hook structure, FlhA$_L$ binds to the D1 and D3 domains of its neighboring subunit, inducing conformational changes of the FlhA$_C$ ring in a highly cooperative manner. As a result, the protein export apparatus terminates the export of the hook protein and initiates the export of filament-type proteins responsible for filament formation at the hook tip.

with the chaperone-substrate complexes (*15*, *16*) but not in FlhA$_C$ ring formation (fig. S7). Therefore, we propose that the interactions of FlhA$_L$ with its neighboring subunit may induce conformational arrangements of the FlhA$_C$ ring in a highly cooperative manner, allowing filament-type substrates in complex with their cognate chaperones to be bound to the FlhA$_C$ ring for their efficient export (Fig. 5).

FliJ binds to FlhA$_L$, allowing the export gate complex to drive flagellar protein export in a PMF-dependent manner (*6*, *30*). FliH and FliI are required for efficient FliJ-FlhA$_L$ interaction (*6*, *27*). Here, the FlhA(L401A) mutations reduced not only the probability of FlhA$_C$ ring formation (Fig. 2D) but also the rate of filament-type protein export (Fig. 3A). The L401A mutation also decreased the binding affinity of FlhA$_C$ for FliJ (Fig. 4A and fig. S5C), suggesting that Leu^{401} is involved in the interaction with FliJ. The L401A mutation totally inhibited the export of FlgK in the absence of FliH and FliI but not in their presence (Fig. 4B). The L401A mutation did not abolish the export of FlgD even in the absence of FliH and FliI (Fig. 4B). In agreement with this, the Δ*fliH-fliI flhB* flhA*(L401A) cells produced the HBBs (fig. S6A). These results suggest that the flagellar type III export gate complex containing FlhA(L401A) requires FliH and FliI to transport filament-type proteins upon completion of the hook structure. Therefore, we propose that FliH and FliI may support efficient interaction between FliJ and FlhA$_L$ to induce structural remodeling of the FlhA$_C$ ring structure through cooperative interactions between FlhA$_{L\text{-}C}$ of each subunit and FlhA$_C$ of its neighboring subunit for the substrate specificity switching of the flagellar protein export apparatus.

MATERIALS AND METHODS

Bacterial strains, plasmids, DNA manipulations, and media

Salmonella strains and plasmids used in this study are listed in table S1. DNA manipulations, site-directed mutagenesis, and DNA sequencing were carried out as described previously (*31*). L-broth and soft agar plates were prepared as described previously (*4*, *5*). Ampicillin was added to the media at a final concentration of 100 μg/ml.

Purification of His-FlhA$_C$ and its mutant variants

His-FlhA$_C$ and its mutant variants were purified by Ni-NTA (nitrilotriacetic acid) affinity chromatography from the soluble fractions of *Escherichia coli* BL21(DE3) (Novagen) cells carrying a pET15b-based plasmid, followed by size-exclusion chromatography with a Superdex 75 column (GE Healthcare) equilibrated with 50 mM tris-HCl (pH 8.0), 100 mM NaCl, 1 mM EDTA, and 1 mM dithiothreitol, as described previously (*22*).

HS-AFM imaging and image analysis

HS-AFM imaging was performed in solution using a laboratory-built HS-AFM setup (*32*, *33*), as described previously (*34*). In brief, a glass sample stage (diameter, 2 mm; height, 2 mm) with a thin mica disc (1 mm in diameter and ~0.05 mm thick) glued to the top by epoxy was attached onto the top of a Z-scanner by a drop of nail polish. A freshly cleaved mica surface was prepared by removing the top layers of mica using a Scotch tape. Then, 2 μl of protein solution with various concentrations in a dilution buffer [50 mM tris-HCl (pH 8.0), 100 mM NaCl] was deposited onto the mica surface. After incubation at room temperature for 3 min, the mica surface was rinsed with 20 μl of an observation buffer [10 mM tris-HCl (pH 6.8)] to remove floating samples. The sample stage was then immersed in a liquid cell containing about 60 μl of the observation buffer. AFM imaging was carried out in a tapping mode, using small cantilevers (BLAC10DS-A2, Olympus) (resonant frequency, ~0.5 MHz in water; quality factor, ~2 in water; spring constant, ~0.1 N/m). The cantilever's free oscillation amplitude A_0 and set-point amplitude A_s were set at 1 to 2 nm and ~0.9 × A_0, respectively.

For AFM image analysis, HS-AFM images were pretreated by a low-pass filter to remove spike noise and a flatten filter to make the overall *xy* plane flat, using a laboratory-built software as described before (*35*). More than 100 individual molecules per frame in each condition were analyzed. The accuracy of our HS-AFM measurements is estimated to be about 1 nm for distance between two objects and 0.15 nm for height (*36*). To simulate HS-AFM images of $FlhA_C$ monomers and the $FlhA_C$ nonamers, we used the software tool, SPM simulator (Advanced Algorithm Systems), as described previously (*24*).

Preparation of mica-supported planar lipid bilayers

Mica-supported planar phospholipid bilayers were prepared as described previously (*34*). Phospholipids used in this study were composed of DPTAP (1,2-dipalmitoyl-3-trimethylammonium-propane), NTA-DPGS (1,2-dipalmitoyl-sn-glycero-3-[(N-(5-amino-1-carboxypentyl)iminodiacetic acid)succinyl]), biotin-cap-DPPE [1,2-dipalmitoyl-sn-glycero-3-phosphoethanolamine-N-(cap biotinyl)], and DPPC (1,2-dipalmitoyl-sn-glycero-3-phosphocholine) (Avanti Polar Lipids Inc.) in a 2.5 to 1 to 1 to 95.5 weight ratio. Chloroform in the lipid mixture was dried up under a stream of N_2 gas and was completely evaporated by a vacuum desiccator. Milli-Q water was added to the dried phospholipid mixture, and the suspension was sonicated to prepare the multilamellar vesicles. The phospholipid mixture was diluted in a 10 mM $MgCl_2$ solution and was sonicated to prepare small unilamellar vesicles. The membrane vesicles were put onto freshly cleaved mica and were incubated for 10 min at room temperature to spread phospholipid bilayers on the mica surface. The surplus vesicles were removed by rinsing with Milli-Q water. A drop of 5 mM $NiCl_2$ solution was deposited onto the phospholipid bilayers, and the stage was incubated for 30 s at room temperature. After washing with an imaging solution, a drop of sample solution was deposited, and then HS-AFM imaging was carried out.

Motility assay in soft agar

Fresh colonies were inoculated onto soft agar plates and incubated at 30°C.

Immunostaining of flagellar filaments

Salmonella cells were attached to a coverslip (Matsunami glass), and unattached cells were washed away with motility medium [10 mM potassium phosphate (pH 7.0), 0.1 mM EDTA, and 10 mM sodium lactate]. Flagellar filaments were labeled with a fluorescent dye, Alexa Fluor 594 (Invitrogen), and were observed by fluorescence microscopy as described previously (*37*).

Secretion assay

Details of sample preparations have been described previously (*38*). After SDS–polyacrylamide gel electrophoresis, immunoblotting with polyclonal anti-FlgD, anti-FlgE, anti-FlgK, anti-FlgL, anti-FlgM, or anti-FliC antibody was carried out as described previously (*4*). Detection was performed with an ECL prime immunoblotting detection kit (GE Healthcare). Chemiluminescence signals were captured by a Luminoimage analyzer LAS-3000 (GE Healthcare). More than three independent experiments were carried out.

Preparation of HBB and measurements of the hook length

HBBs were prepared as described previously (*39*). After sucrose density gradient ultracentrifugation, samples containing HBBs and intact flagella were collected from a 20 to 50% sucrose density gradient in 10 mM tris-HCl (pH8.0), 5 mM EDTA, and 1% Triton X-100. After ultracentrifugation of fractions containing the HBBs at 60,000*g* for 60 min, the pellets were resuspended in 50 μl of a TET (Tris EDTA Triton) buffer [10 mM tris-HCl (pH 8.0), 5 mM EDTA, 0.1% Triton X-100]. When intact flagella were prepared from the sucrose density gradient, followed by ultracentrifugation at 60,000*g* for 60 min, the pellets were suspended in 50 mM glycine (pH 2.5) and 0.1% Triton X-100 and were incubated at room temperature for 30 min to depolymerize the flagellar filaments. After ultracentrifugation, the pellets were resuspended in 50 μl of the TET buffer. Samples were negatively stained with 2% uranyl acetate. Electron micrographs were recorded with a JEM-1011 transmission electron microscope (JEOL) operated at 100 kV and equipped with an F415 charge-coupled device camera (TVIPS) at a magnification of ×5500, which corresponds to 2.75 nm per pixel. Hook length was measured by ImageJ version 1.48 (National Institutes of Health).

Pull-down assays by GST chromatography

Detail protocols for pull-down assays by GST affinity chromatography have been described previously (*6*, *16*). At least three independent experiments were carried out.

SUPPLEMENTARY MATERIALS

Supplementary material for this article is available at http://advances.sciencemag.org/cgi/content/full/4/4/eaao7054/DC1

fig. S1. Comparison of experimental HS-AFM image of an $FlhA_C$ monomer with a simulated AFM image of the crystal structure of $FlhA_C$.
fig. S2. Effect of phospholipids on $FlhA_C$ ring formation.
fig. S3. Effect on motility and flagellar formation of alanine substitutions of residues involved in interactions of $FlhA_L$ with its neighboring subunit in the $FlhA_C$ crystal.
fig. S4. Effect of phospholipids on ring formation of $FlhA_C$ mutant variants.
fig. S5. Effect of FlhA mutations on interactions of $FlhA_C$ with FlgN and FliJ.
fig. S6. Effect of depletion of FliH and FliI on the export function of FlhA(L401A).
fig. S7. Effect of the FlhA(F459A) mutation on $FlhA_C$ ring formation.
table S1. *Salmonella* strains and plasmids used in this study.
movie S1. Real-time imaging of $FlhA_C$ ring assembly on mica.
movie S2. Typical HS-AFM imaging of wild-type $FlhA_C$ placed on mica surface.
movie S3. Typical HS-AFM imaging of $FlhA_C$38K placed on mica surface.
movie S4. Typical HS-AFM imaging of wild-type $FlhA_C$ placed on mica-supported planar phospholipid bilayers.
movie S5. Typical HS-AFM imaging of $FlhA_C$38K placed on mica-supported planar phospholipid bilayers.
References (*40*–*45*)

REFERENCES AND NOTES

1. F. F. V. Chevance, K. T. Hughes, Coordinating assembly of a bacterial macromolecular machine. *Nat. Rev. Microbiol.* **6**, 455–465 (2008).
2. T. Minamino, Protein export through the bacterial flagellar type III export pathway. *Biochim. Biophys. Acta* **1843**, 1642–1648 (2014).
3. M. Kinoshita, S.-I. Aizawa, Y. Inoue, K. Namba, T. Minamino, The role of intrinsically disordered C-terminal region of FliK in substrate specificity switching of the bacterial flagellar type III export. *Mol. Microbiol.* **105**, 572–588 (2017).
4. T. Minamino, R. M. Macnab, Components of the *Salmonella* flagellar export apparatus and classification of export substrates. *J. Bacteriol.* **181**, 1388–1394 (1999).
5. T. Minamino, R. M. Macnab, Interactions among components of the *Salmonella* flagellar export apparatus and its substrates. *Mol. Microbiol.* **35**, 1052–1064 (2000).
6. T. Minamino, Y. V. Morimoto, N. Hara, K. Namba, An energy transduction mechanism used in bacterial flagellar type III protein export. *Nat. Commun.* **2**, 475 (2011).
7. Y. V. Morimoto, N. Kami-ike, T. Miyata, A. Kawamoto, T. Kato, K. Namba, T. Minamino, High-resolution pH imaging of living bacterial cell to detect local pH differences. *mBio* **7**, e01911–e16 (2016).
8. T. Minamino, Y. V. Morimoto, N. Hara, P. D. Aldridge, K. Namba, The bacterial flagellar Type III export gate complex is a dual fuel engine that can use both H^+ and Na^+ for flagellar protein export. *PLOS Pathog.* **12**, e1005495 (2016).
9. M. Erhardt, P. Wheatley, E. A. Kim, T. Hirano, Y. Zhang, M. K. Sarkar, K. T. Hughes, D. F. Blair, Mechanism of type-III protein secretion: Regulation of FlhA conformation by a functionally critical charged-residue cluster. *Mol. Microbiol.* **104**, 234–249 (2017).
10. P. Abrusci, M. Vergara-Irigaray, S. Johnson, M. D. Beeby, D. R. Hendrixson, P. Roversi, M. E. Friede, J. E. Deane, G. J. Jensen, C. M. Tang, S. M. Lea, Architecture of the major component of the type III secretion system export apparatus. *Nat. Struct. Mol. Biol.* **20**, 99–104 (2013).
11. A. Kawamoto, Y. V. Morimoto, T. Miyata, T. Minamino, K. T. Hughes, T. Kato, K. Namba, Common and distinct structural features of *Salmonella* injectisome and flagellar basal body. *Sci. Rep.* **3**, 3369 (2013).
12. Y. V. Morimoto, M. Ito, K. D. Hiraoka, Y.-S. Che, F. Bai, N. Kami-ike, K. Namba, T. Minamino, Assembly and stoichiometry of FliF and FlhA in *Salmonella* flagellar basal body. *Mol. Microbiol.* **91**, 1214–1226 (2014).
13. Y. Saijo-Hamano, K. Imada, T. Minamino, M. Kihara, M. Shimada, A. Kitao, K. Namba, Structure of the cytoplasmic domain of FlhA and implication for flagellar type III protein export. *Mol. Microbiol.* **76**, 260–268 (2010).
14. G. Bange, N. Kümmerer, C. Engel, G. Bozkurt, K. Wild, I. Sinning, FlhA provides the adaptor for coordinated delivery of late flagella building blocks to the type III secretion system. *Proc. Natl. Acad. Sci. U.S.A.* **107**, 11295–11300 (2010).
15. T. Minamino, M. Kinoshita, N. Hara, S. Takeuchi, A. Hida, S. Koya, H. Glenwright, K. Imada, P. D. Aldridge, K. Namba, Interaction of a bacterial flagellar chaperone FlgN with FlhA is required for efficient export of its cognate substrates. *Mol. Microbiol.* **83**, 775–788 (2012).
16. M. Kinoshita, N. Hara, K. Imada, K. Namba, T. Minamino, Interactions of bacterial flagellar chaperone-substrate complexes with FlhA contribute to co-ordinating assembly of the flagellar filament. *Mol. Microbiol.* **90**, 1249–1261 (2013).
17. M. Kinoshita, Y. Nakanishi, Y. Furukawa, K. Namba, K. Imada, T. Minamino, Rearrangements of α-helical structures of FlgN chaperone control the binding affinity for its cognate substrates during flagellar type III export. *Mol. Microbiol.* **101**, 656–670 (2016).
18. Y. Furukawa, Y. Inoue, A. Sakaguchi, Y. Mori, T. Fukumura, T. Miyata, K. Namba, T. Minamino, Structural stability of flagellin subunit affects the rate of flagellin export in the absence of FliS chaperone. *Mol. Microbiol.* **102**, 405–416 (2016).
19. C. S. Barker, T. Inoue, I. V. Meshcheryakova, S. Kitanobo, F. A. Samatey, Function of the conserved FHIPEP domain of the flagellar type III export apparatus, protein FlhA. *Mol. Microbiol.* **100**, 278–288 (2016).
20. N. Hartmann, D. Büttner, The inner membrane protein HrcV from *Xanthomonas* spp. is involved in substrate docking during type III secretion. *Mol. Plant Microbe Interact.* **26**, 1176–1189 (2013).
21. T. Hirano, S. Mizuno, S.-I. Aizawa, K. T. Hughes, Mutations in FlK, FlgG, FlhA, and FlhE that affect the flagellar type III secretion specificity switch in *Salmonella enterica*. *J. Bacteriol.* **191**, 3938–3949 (2009).
22. Y. Saijo-Hamano, T. Minamino, R. M. Macnab, K. Namba, Structural and functional analysis of the C-terminal cytoplasmic domain of FlhA, an integral membrane component of the type III flagellar protein export apparatus in *Salmonella*. *J. Mol. Biol.* **343**, 457–466 (2004).
23. N. Kodera, D. Yamamoto, R. Ishikawa, T. Ando, Video imaging of walking myosin V by high-speed atomic force microscopy. *Nature* **468**, 72–76 (2010).
24. T. Uchihashi, R. Iino, T. Ando, H. Noji, High-speed atomic force microscopy reveals rotary catalysis of rotorless F_1-ATPase. *Science* **333**, 755–758 (2011).
25. N. Terahara, N. Kodera, T. Uchihashi, T. Ando, K. Namba, T. Minamino, Na^+-induced structural transition of MotPS for stator assembly of the *Bacillus* flagellar motor. *Sci. Adv.* **3**, eaao4119 (2017).
26. K. T. Hughes, K. L. Gillen, M. J. Semon, J. E. Karlinsey, Sensing structural intermediates in bacterial flagellar assembly by export of a negative regulator. *Science* **262**, 1277–1280 (1993).
27. T. Minamino, M. Kinoshita, Y. Inoue, Y. V. Morimoto, K. Ihara, S. Koya, N. Hara, N. Nishioka, S. Kojima, M. Homma, K. Namba, FliH and FliI ensure efficient energy coupling of flagellar type III protein export in *Salmonella*. *Microbiologyopen* **5**, 424–435 (2016).
28. T. Minamino, K. Namba, Distinct roles of the FliI ATPase and proton motive force in bacterial flagellar protein export. *Nature* **451**, 485–488 (2008).
29. Y. Inoue, Y. V. Morimoto, K. Namba, T. Minamino, Novel insights into the mechanism of well-ordered assembly of bacterial flagellar proteins in *Salmonella*. *Sci. Rep.* **8**, 1787 (2018).
30. T. Ibuki, Y. Uchida, Y. Hironaka, K. Namba, K. Imada, T. Minamino, Interaction between FliJ and FlhA, components of the bacterial flagellar type III export apparatus. *J. Bacteriol.* **195**, 466–473 (2013).
31. N. Hara, K. Namba, T. Minamino, Genetic characterization of conserved charged residues in the bacterial flagellar type III export protein FlhA. *PLOS ONE* **6**, e22417 (2011).
32. T. Ando, N. Kodera, E. Takai, D. Maruyama, K. Saito, A. Toda, A high-speed atomic force microscope for studying biological macromolecules. *Proc. Natl. Acad. Sci. U.S.A.* **98**, 12468–12472 (2001).
33. T. Ando, T. Uchihashi, T. Fukuma, High-speed atomic force microscopy for nano-visualization of dynamic biomolecular processes. *Prog. Surf. Sci.* **83**, 337–437 (2008).
34. T. Uchihashi, N. Kodera, T. Ando, Guide to video recording of structure dynamics and dynamic processes of proteins by high-speed atomic force microscopy. *Nat. Protoc.* **7**, 1193–1206 (2012).
35. K. X. Ngo, N. Kodera, E. Katayama, T. Ando, T. Q. P. Uyeda, Cofilin-induced unidirectional cooperative conformational changes in actin filaments revealed by high-speed atomic force microscopy. *eLife* **4**, e04806 (2015).
36. M. Hashimoto, N. Kodera, Y. Tsunaka, M. Oda, M. Tanimoto, T. Ando, K. Morikawa, S.-. Tate, Phosphorylation-coupled intramolecular dynamics of unstructured regions in chromatin remodeler FACT. *Biophys. J.* **104**, 2222–2234 (2013).
37. T. Minamino, Y. V. Morimoto, M. Kinoshita, P. D. Aldridge, K. Namba, The bacterial flagellar protein export apparatus processively transports flagellar proteins even with extremely infrequent ATP hydrolysis. *Sci. Rep.* **4**, 7579 (2014).
38. T. Minamino, M. Kinoshita, K. Namba, Fuel of the bacterial flagellar type III protein export apparatus. *Methods Mol. Biol.* **1593**, 3–16 (2017).
39. K. D. Hiraoka, Y. V. Morimoto, Y. Inoue, T. Fujii, T. Miyata, F. Makino, T. Minamino, K. Namba, Straight and rigid flagellar hook made by insertion of the FlgG specific sequence into FlgE. *Sci. Rep.* **7**, 46723 (2017).
40. K. Ohnishi, Y. Ohto, S. Aizawa, R. M. Macnab, T. Iino, FlgD is a scaffolding protein needed for flagellar hook assembly in *Salmonella typhimurium*. *J. Bacteriol.* **176**, 2272–2281 (1994).
41. N. Hara, Y. V. Morimoto, A. Kawamoto, K. Namba, T. Minamino, Interaction of the extreme N-terminal region of FliH with FlhA is required for efficient bacterial flagellar protein export. *J. Bacteriol.* **194**, 5353–5360 (2012).
42. K. Ohnishi, F. Fan, G. J. Schoenhals, M. Kihara, R. M. Macnab, The FliO, FliP, FliQ, and FliR proteins of *Salmonella typhimurium*: Putative components for flagellar assembly. *J. Bacteriol.* **179**, 6092–6099 (1997).
43. Y. Furukawa, K. Imada, F. Vonderviszt, H. Matsunami, K.-i. Sano, K. Kutsukake, K. Namba, Interactions between bacterial flagellar axial proteins in their monomeric state in solution. *J. Mol. Biol.* **318**, 889–900 (2002).
44. M. Kihara, T. Minamino, S. Yamaguchi, R. M. Macnab, Intergenic suppression between the flagellar MS ring protein FliF of *Salmonella* and FlhA, a membrane component of its export apparatus. *J. Bacteriol.* **183**, 1655–1662 (2001).
45. T. Minamino, M. Shimada, M. Okabe, Y. Saijo-Hamano, K. Imada, M. Kihara, K. Namba, Role of the C-terminal cytoplasmic domain of FlhA in bacterial flagellar type III protein export. *J. Bacteriol.* **192**, 1929–1936 (2010).

Acknowledgments: We thank M. Kinoshita for critical reading of the manuscript and helpful comments. **Funding:** This research has been supported in part by the Japan Society for the Promotion of Science KAKENHI (grant numbers JP15H04360 to N.K., JP15K14498 and JP15H05593 to Y.V.M., JP15H03540 to T.U., JP15H02386 to K.I., JP24227005 to T.A., JP25000013 to K.N., and JP26293097 to T.M.), the Ministry of Education, Culture, Sports, Science and Technology KAKENHI (grant numbers JP26115720 and JP15H01335 to Y.V.M., JP26119003 to T.A., and JP24117004 and JP15H01640 to T.M.), and the Japan Science and Technology Agency (grant numbers JPMJPR13L4 to N.K. and JPMJCR13M1 to T.A.). **Author contributions:** K.N. and T.M. conceived and designed the research. N.T., Y.I., N.K., Y.V.M., and T.M. preformed the research. N.K., T.U., and T.A. set up the HS-AFM imaging system (both hardware and software). N.T., Y.I., N.K., Y.V.M., T.U., K.I., and T.M. analyzed the data. K.N. and T.M. wrote the paper based on discussion with other authors. **Competing interests:** The authors declare that they have no competing interests. **Data and materials availability:** All data needed to evaluate the conclusions in the paper are present in the paper and/or the Supplementary Materials. Additional data related to this paper may be requested from the authors.

Submitted 17 August 2017
Accepted 9 March 2018
Published 25 April 2018
10.1126/sciadv.aao7054

Citation: N. Terahara, Y. Inoue, N. Kodera, Y. V. Morimoto, T. Uchihashi, K. Imada, T. Ando, K. Namba, T. Minamino, Insight into structural remodeling of the FlhA ring responsible for bacterial flagellar type III protein export. *Sci. Adv.* **4**, eaao7054 (2018).